MID-AMERICA TRANSPORTATION CENTER

Report # MATC-UI: 142-4

Final Report
WBS: 25-1121-0005-142-4

Infrastructure Inspection During and After Unexpected Events - Phase IV

Salam Rahmatalla, PhD
Professor
Department of Civil and Environmental Engineering
The University of Iowa

Casey Harwood, PhD
Assistant Professor
Department of Mechanical Engineering
The University of Iowa

Ali Karimpour, PhD
Postdoctoral Research Scholar
Department of Civil and Environmental Engineering
The University of Iowa

2021

A Cooperative Research Project sponsored by
U.S. Department of Transportation- Office of the Assistant Secretary for Research and Technology

MATC

Infrastructure Inspection During and After Unexpected Events – Phase IV

Salam Rahmatalla, PhD
Professor
Civil and Environmental Engineering
University of Iowa

Ali Karimpour, PhD
Postdoctoral Research Scholar
Civil and Environmental Engineering
University of Iowa

Casey Harwood, PhD
Assistant Professor
Mechanical Engineering
University of Iowa

A Report on Research Sponsored by

Mid-America Transportation Center

University of Nebraska-Lincoln

January 2022

Technical Report Documentation Page

1. Report No. WBS no. 25-1121-0005-142-4	**2. Government Accession No.**	**3. Recipient's Catalog No.**	
4. Title and Subtitle Infrastructure Inspection During and After Unexpected Events Fourth Year Final Report and Outcomes		**5. Report Date** December 2021	
		6. Performing Organization Code	
7. Author(s) Salam Rahmatalla, PhD ORCID: 0000-0003-3889-4364 Ali Karimpour, PhD Casey Harwood, PhD		**8. Performing Organization Report No.** 25-1121-0005-142-4	
9. Performing Organization Name and Address Mid-America Transportation Center 2200 Vine St. PO Box 830851 Lincoln, NE 68583-0851		**10. Work Unit No. (TRAIS)**	
		11. Contract or Grant No. 69A3551757107	
12. Sponsoring Agency Name and Address		**13. Type of Report and Period Covered** Final Report December 2020 – December 2021	
		14. Sponsoring Agency Code MATC TRB Rip No. 91994-80	
15. Supplementary Note			

16. Abstract

This report compares the performance of a representative highway bridge with two different bearing systems under extreme flood events. A numerical model of the representative highway bridge with a conventional roller/rocker bearing system was compared to the same bridge model but with a newly integral abutment bearing system. Both scenarios were successfully modeled, and their outcomes clarify failure modes of common highway bridge systems against extreme flood conditions. The first and most important outcome of this study indicates that a bridge with an integral abutment system would tolerate much more severe flood intensity than the same bridge with a conventional bearing system. Secondly, the complicity of the failure mode for integral abutment indicates that there are several completely plastic spots/hinges rather than a single failure mode. Therefore, it seems that more research studies are required in order to categorize such bridge structural systems, which are classified based on their span lengths. The current research study was performed on a small-span representative bridge.

17. Key Words Structural Failure Mode, Finite Element Model (FEM), Highway Bridges, Integral Abutment System.		**18. Distribution Statement**	
19. Security Class if. (Of this report) Unclassified	**20. Security Class if. (Of this page)** Unclassified	**21. No. of Pages** 16	**22. Price**

Table of Contents

List of Figures

Disclaimer

The contents of this report reflect the views of the authors, who are responsible for the facts and the accuracy of the information presented herein. This document is disseminated under the sponsorship of the U.S. Department of Transportation's University Transportation Centers Program, in the interest of information exchange. The U.S. Government assumes no liability for the contents or use thereof.

Executive Summary

This report investigates the performance assessment of highway bridges with conventional and integral abutments against extreme flooding events. Several numerical simulations have been carried out to examine these bridge behaviors during flooding. In the new integral abutment system, which was introduced during recent decades, bridge superstructures are constructed as integral parts of the substructures using high-performance concrete material. The results showed the integral abutment system demonstrated high resistance to lateral flood loading. This could be because integral abutment systems are not vulnerable to the dislodging failure mode that affects conventional bearing systems. While this study indicates that integral abutment systems can experience more complicated modes of failure, more research is needed to completely understand their behaviors under extreme flooding events in vulnerable areas.

Chapter 1 Introduction and Background

After Hurricane Ivan in 2004 and Hurricanes Katrina and Rita in 2005, the Federal Highway Administration (FHWA) initiated a research project and assigned funding to publish guidelines for bridge owners in areas vulnerable to flooding (Kulicki 2010). The final product is AASHTO's *Guide Specifications for Bridges Vulnerable to Coastal Storms* (AASHTO 2008). The prevalent failure mode of highway bridges in flood-prone zones is attributed to a dislodging and unseating phenomenon in which bridge spans are pushed away from their original locations and eventually drop into their conduits (Padgett et al. 2012; Ataei & Padgett 2013a; Azadbakht & Yim 2015). In addition to the unseating failure modes in simply supported span bridges, other types of failure modes across various bearing systems should be investigated (Ataei & Padgett 2013b; Saeidpour et al. 2018).

This report studies the performance of a representative highway bridge with a newly developed bearing system (integral abutment/pier caps) and compares it to the same model with a conventional bearing system. After constructing a comprehensive numerical model of the representative bridge, the loading patterns extracted from AASHTO code are imposed on it. Failure modes and extreme stress levels in various bridge components (concrete deck, rebar, girders, and stringers) are investigated.

Chapter 2 Hydrodynamic Loading to Vulnerable Bridges

There are several simplified methods in the literature that can be exploited with high reliability to calculate the storm surge loads on the bridge superstructures (Yim & Azadbakht 2013; Azadbakht & Yim 2015; Azadbakht & Yim 2016). These simplified methods separate the impact of storm surges upon the bridge superstructures into two incident stages: (1) initial impact and overtopping flow over the deck, and (2) full inundation. The parametric simplified formulas are expressed as follows:

$$F_{H_{max}} = F_{h\_hs} + F_d = 0.5\gamma_w h_0^2 + 0.5C_d\rho_w v^2 h_0; \qquad h_0 < L_h \tag{2.1}$$

$$F_{H_{max}} = F_{h\_hs} + F_d = 0.5\gamma_w(2h_0 - L_h)L_h + 0.5C_d\rho_w v^2 L_h; \qquad h_0 \geq L_h \tag{2.2}$$

$$F_{DV_{max}} = C_{DV}\left(F_{v\_hs} + F_{v\_s}\right) = C_{DV}\left[\gamma_w\left(h_0 - L_g - T_d\right)L_v + 0.5C_{v_s}\rho_w v^2 L_{sb}\right] \tag{2.3}$$

$$F_{UP_{max}} = C_{UP}(F_b + F_l) = C_{UP}[\gamma_w V + 0.5C_l\rho_w v^2 L_v] \tag{2.4}$$

where $F_{H_{max}}$, $F_{DV_{max}}$, and $F_{UP_{max}}$ are maximum horizontal force, maximum downward vertical force, and maximum uplift force, respectively. Also, C_d, C_l, C_{v_s}, C_{DV}, and C_{UP} are the drag coefficient, lift coefficient, slamming coefficient in the vertical direction, empirical downward vertical force coefficient, and empirical uplift force coefficient, respectively. $F_{h_{hs}}$, $F_{v_{hs}}$, F_{v_s}, F_d, F_b, and F_l are the hydrostatic horizontal force, hydrostatic downward vertical force, slamming vertical force, drag force, buoyancy force, and lift force, respectively. γ_w, $\rho_w = 2slug/ft^3$, g, V, and v are specific weight of water, density of water, acceleration of gravity, volume of the bridge per 1-ft length, and storm flow velocity, respectively. The other geometric parameters are shown in figure 2.1, and $L_{sb} = 4L_b$.

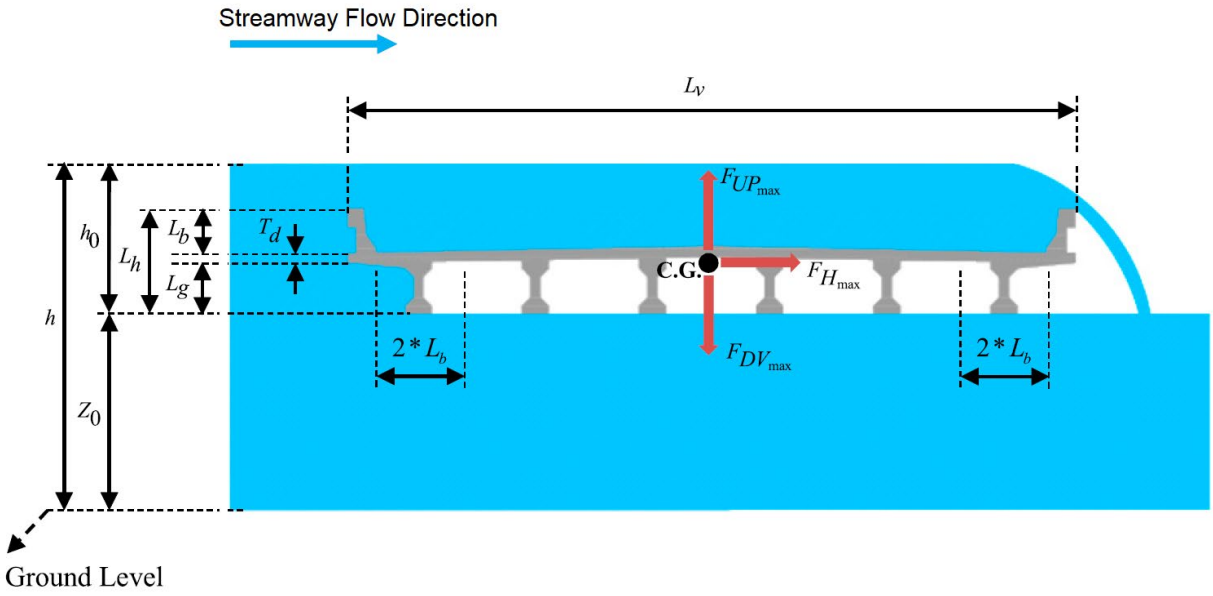

Figure 2.1 Bridge superstructure cross-section schematic with prescribed geometric parameters and imposed load directions.

Chapter 3 Numerical Modeling of Bridge

A representative bridge was selected to be a single-span bridge, which sits on a conventional bearing support over an active streamway in the state of Iowa with an FHWA number of 31690, shown in figure 3.1. As-built detailed plans and records of the bridge geometry plus its material information were collected from the Iowa Department of Transportation and then used to construct a finite element (FE) model of the testbed.

Figure 3.1 Real FHWA 31690 bridge superstructure and its numerical model simulated in Abaqus.

The bridge model was simulated using Abaqus® software (Dassault Systèmes Simulia, 2021). Full composite action between the concrete slab and girders was imposed by a surface-to-surface contact algorithm, while the multipoint constraint algorithm was used to connect bridge components. The concrete body was modeled with a 3D 8-node iso-parametric element (C3D8R), and the reinforcement rebars were modeled as a 3D wire truss element member (T3D2) plus embedded-region constraints inside the concrete medium. The steel cross beams and girders were modeled with eight nodal points, six degrees of freedom, and a reduced integration shell element (S8R). The mesh sensitivity analysis was carried out in order to obtain an acceptable mesh size in which all initial 25 natural frequencies varied by less than 1%.

The numerical properties of the conventional bearing system, rocker and roller bearing systems, plus their associate limit-states were selected from the literature (Pan et al. 2007; Pan et al. 2010) as shown in figure 3.2. For the integral abutment system, the bridge model was fixed by encastre constraints plus embedment length, which are buried inside a concrete medium.

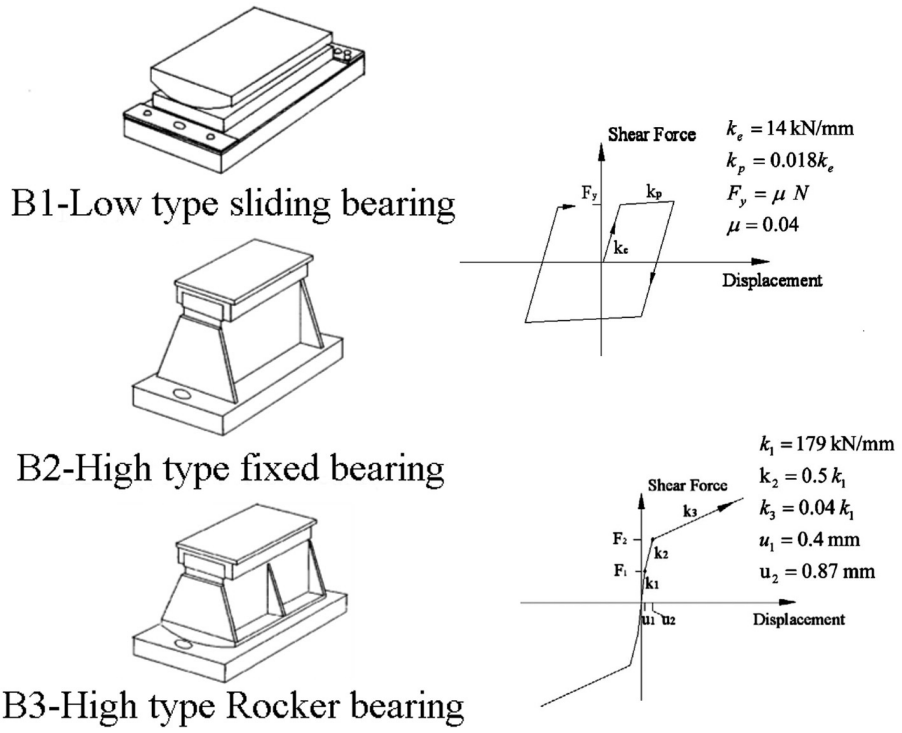

Figure 3.2 Conventional roller (low type and high type) and rocker bearing used as bridge supports.

Chapter 4 Results

4.1 Conventional Bearing System

The conventional bearing system of the bridge under the simulated flood loading responded as expected by undergoing an unseating phenomenon, as shown in figure 4.1. The individual structural components at the moment of failure are shown in figures 4.2 through 4.5. Based on what can be seen in the latter figures, the maximum stress levels of all components at the instant of unseating happened at midspan; also, inclined plastic hinges are initiated around the end-span of the exterior girders as shown in figure 4.5.

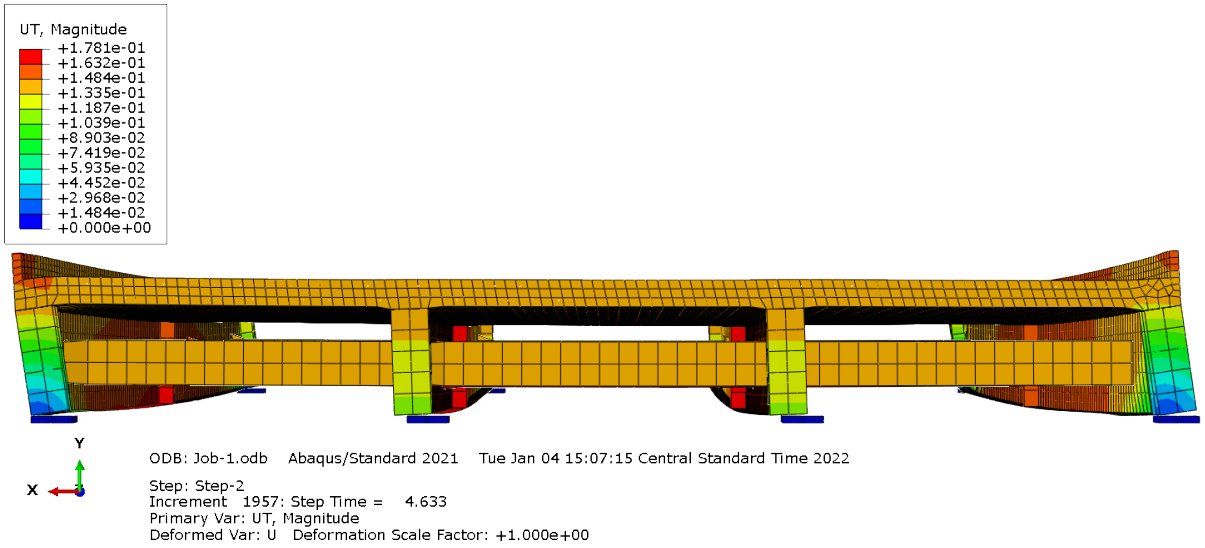

Figure 4.1 Bridge superstructure cross-section view with conventional roller and rocker bearing; its performance with excess drift unseated it from the pedestals.

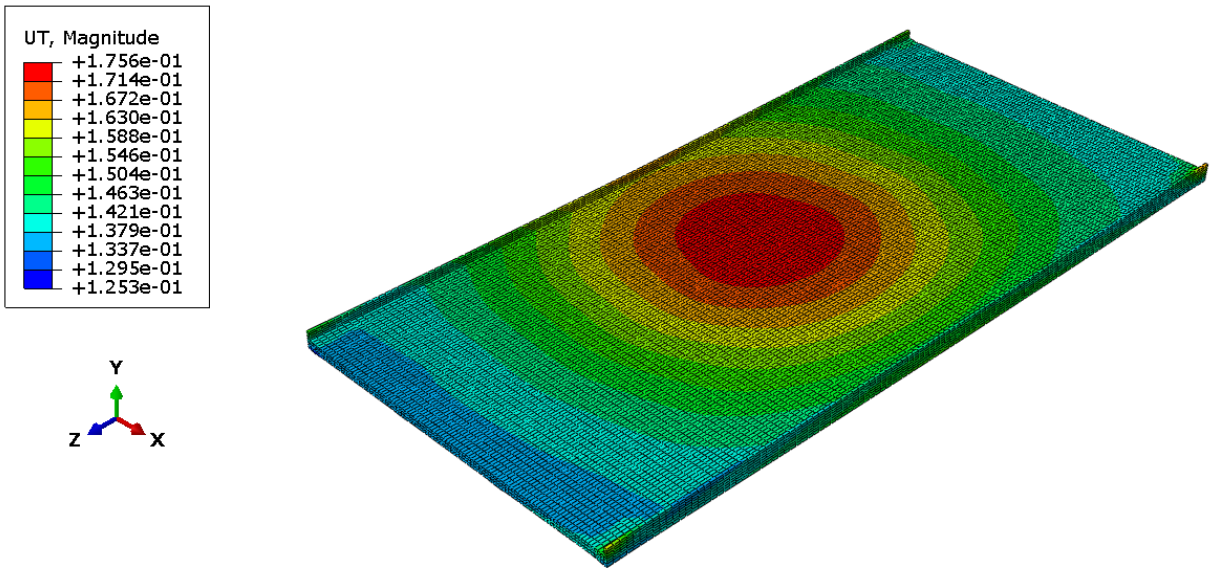

Figure 4.2 Bridge with conventional roller and rocker bearing; maximum bridge displacement at failure moment.

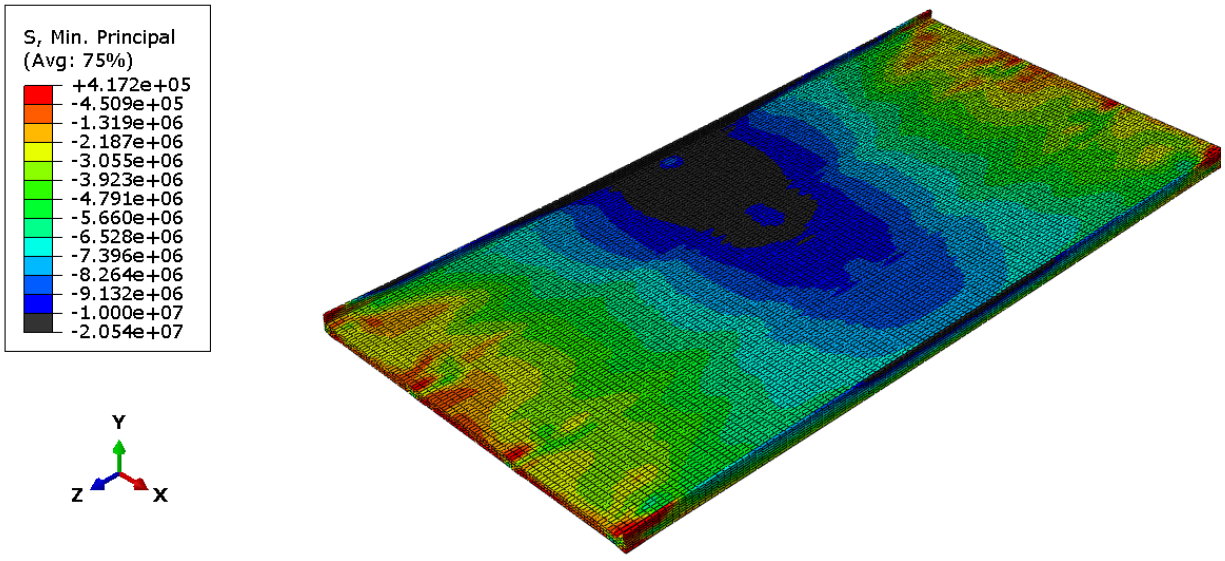

Figure 4.3 Bridge with conventional roller and rocker bearing; maximum concrete deck stress level at failure moment.

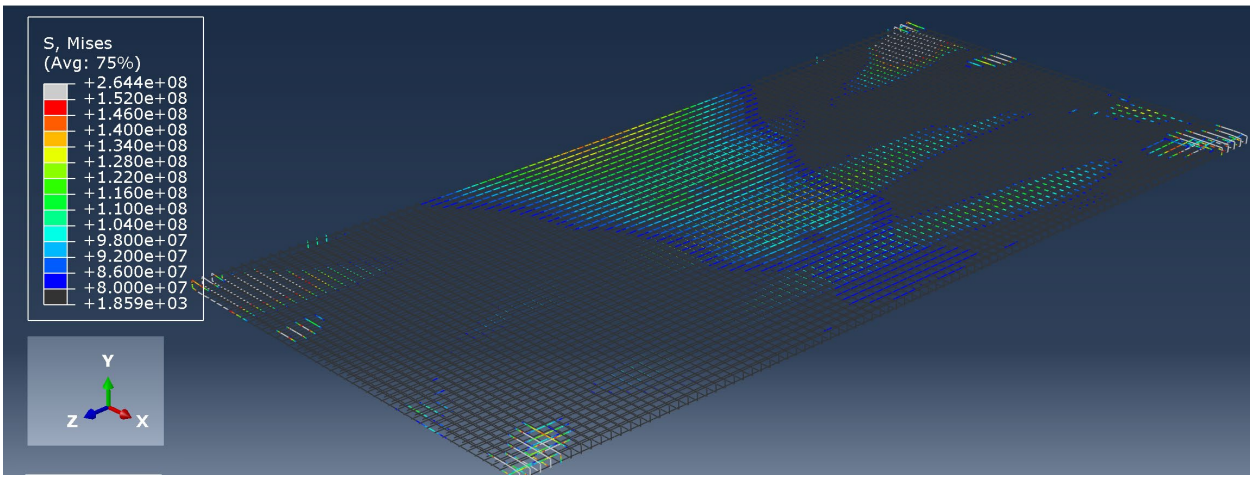

Figure 4.4 Bridge with conventional roller and rocker bearing; maximum rebars stress level at failure moment.

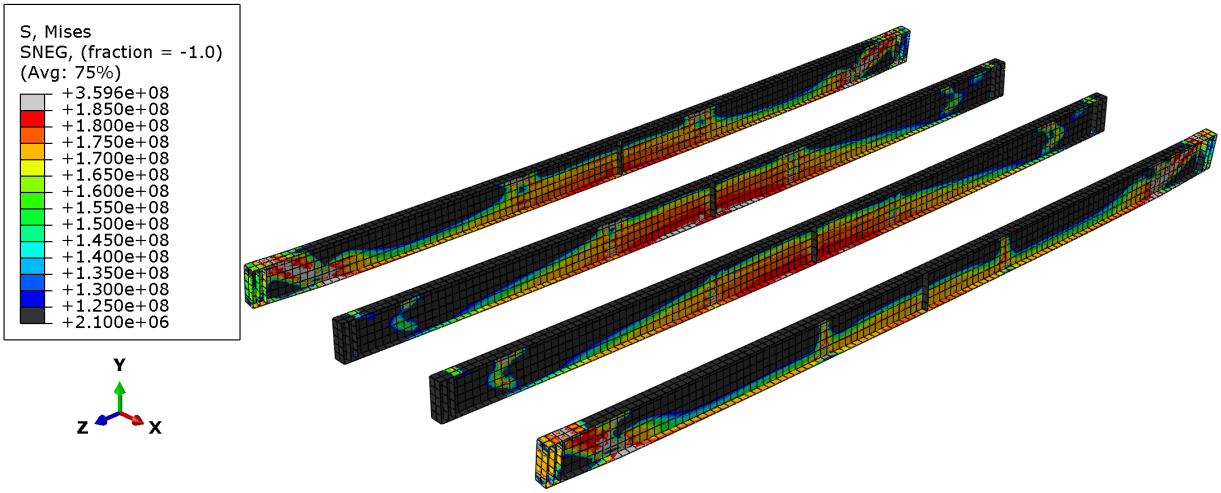

Figure 4.5 Bridge with conventional roller and rocker bearing; maximum girders stress level at failure moment.

4.2 Integral abutment system

In the second scenario, the conventional bearing systems were substituted by the integral abutment, in which the bridge end-span is embedded into the concrete body in practice. Bridge end-span elements were constrained with encastre boundary conditions with predefined embedded lengths, which would be integrated with the abutment concrete in practice. The

displacement around the end-span of the bridge with various maximum stress spots in its components is shown in figures 4.6 through 4.10. The deflections of the bridge deck are reduced substantially, as are the peak stresses in the girders.

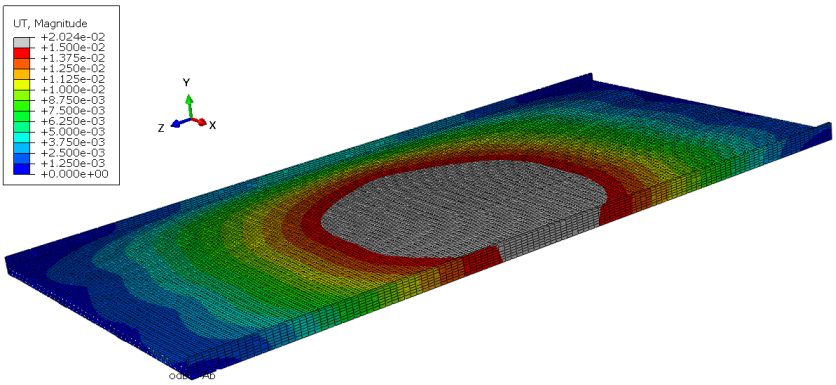

Figure 4.6 Bridge with integral abutment system; concrete deck displacement at failure moment.

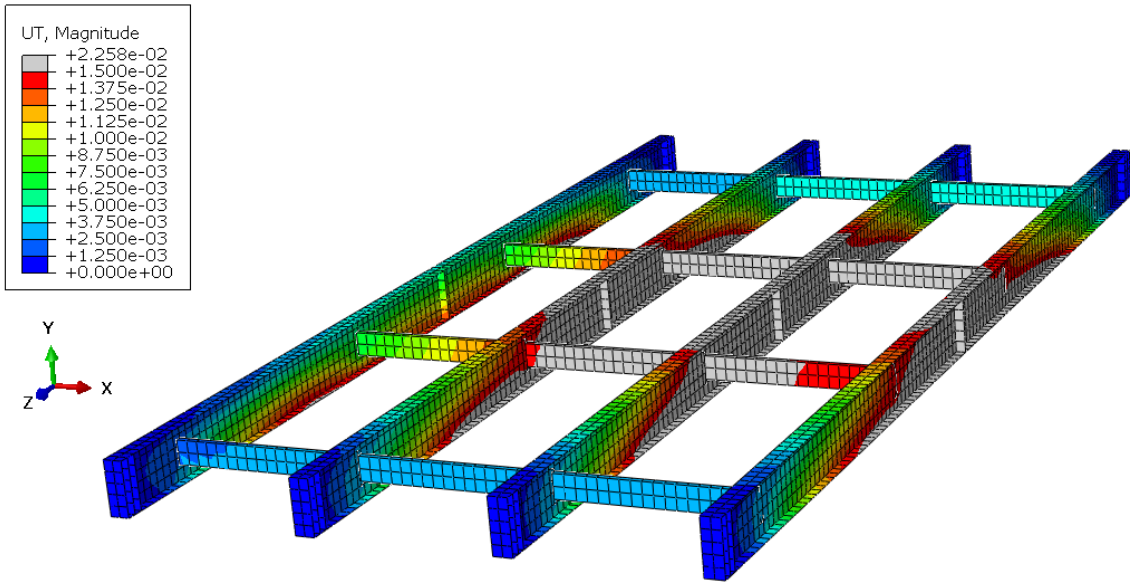

Figure 4.7 Bridge with integral abutment system; maximum bridge girders displacement at failure moment.

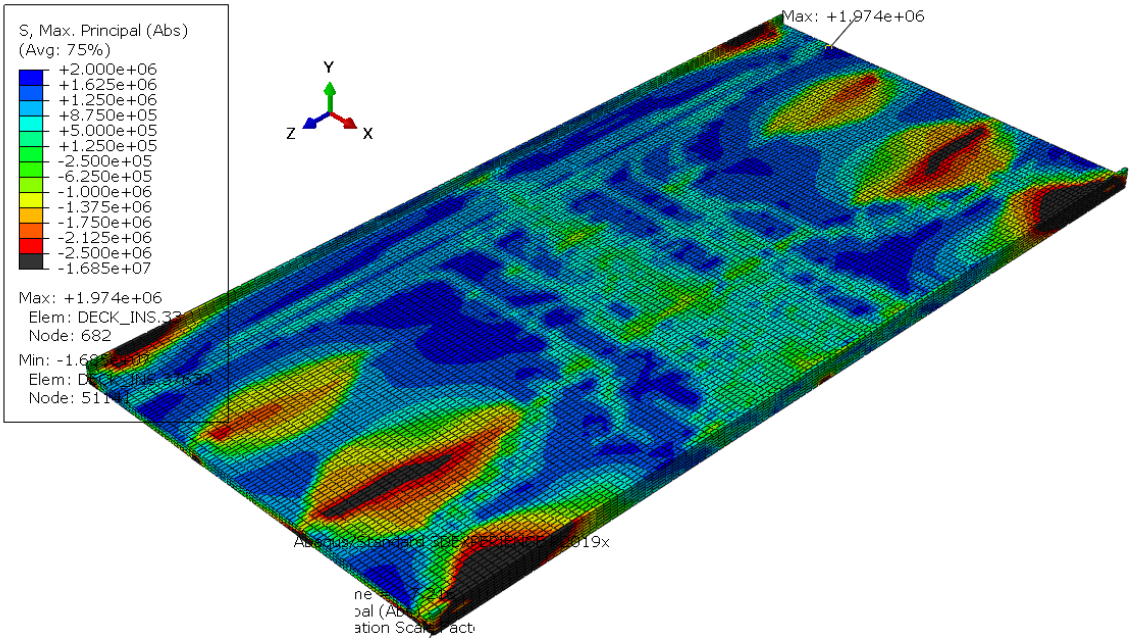

Figure 4.8 Bridge with integral abutment system; maximum concrete deck stress level at failure moment.

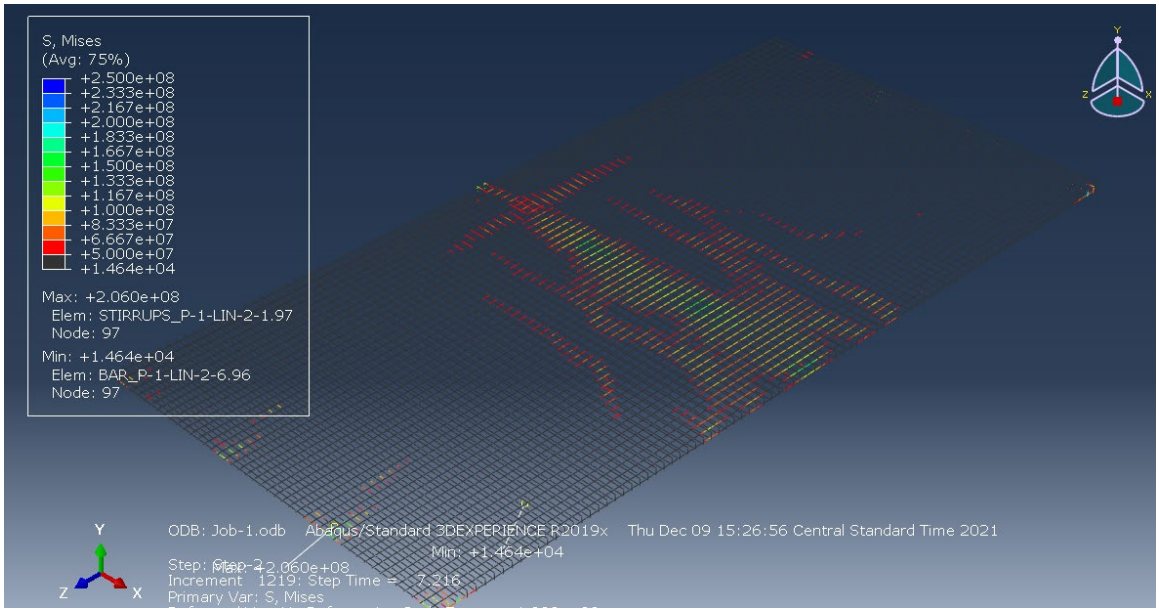

Figure 4.9 Bridge with integral abutment system; maximum rebars stress level at failure moment.

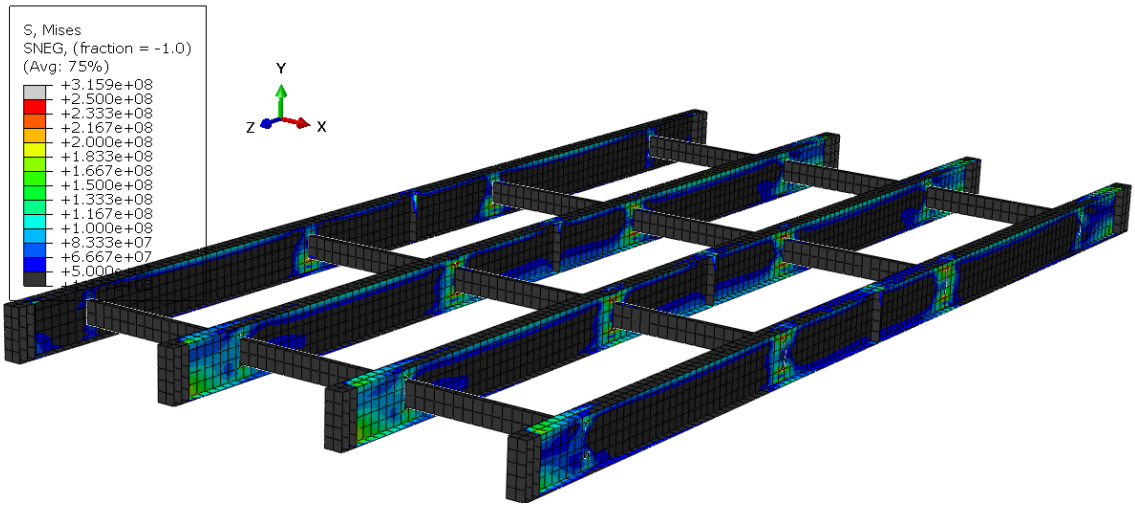

Figure 4.10 Bridge with integral abutment system; maximum girders stress level at failure moment.

Chapter 5 Conclusion

This report studies the behavior of a common type of highway bridge under extreme flooding incidents, focusing on the effects of the bearing system of the bridge during failure mode. To do so, a representative highway bridge was selected, and its numerical model was simulated in a robust software package (Abaqus). Extreme flood loadings were imposed on the bridge to capture when and where each bridge component would fail. Two numerical bridge models, one with a conventional rocker-roller system and one with an integral abutment system, were defined in the software. The unseating phenomenon of the conventional bridge bearing system was observed, while excess deflection from the pedestal/baseplates that would cause dislodging in practice can be clearly seen in the figures of Section (4.1). For this system, the bridge model experiences excessive stress levels at the midspan, where all concrete deck, rebars, and girders reach their associated yielding stress in a manner similar to a simply supported beam loaded laterally and uniformly.

The integral abutment system demonstrated higher resistance to lateral flood loadings but behaved in a more complicated way under extreme flood loadings. In this case, different structural components surpass their associated yielding stress in various locations along the bridge span length. This means that rather than a single failure mode, several failure patterns would be possible. For such a system, as shown in Section (4.2), steel girders and embedded rebar fail around the midspan, initiating a failing domain that starts from the flood angle of attack (right to left). The concrete deck fails at the end-span over the girders, as shown in figure 4.8. Also, the connections between the girders and stringers have most likely experienced plastic hinges, as plotted in figure 4.9. Due to the excessive plasticity in the numerical model in various

spots, the failure mechanism could be initiated by any of the numerous plastic hinges scattered along the bridge superstructure.

The greatest obstacle to future research on such systems lies in the considerable demand upon computer processors to run numerical models with many nonlinearities incorporated and with high accuracy demands. This bridge is categorized as a small span length. Several numerical simulations are ongoing to investigate moderate span length and large span length models. However, due to the nature of the problem and the need for accuracy and nonlinearities incorporated in the study, much more investigation is required to completely understand bridge structural behaviors during extreme flooding events.

References

AASHTO, 2008. Guide specifications for bridges vulnerable to coastal storms, 1st Ed., AASHTO, Washington, DC.

Ataei, N. and Padgett, J.E., 2013a. Limit state capacities for global performance assessment of bridges exposed to hurricane surge and wave. Structural Safety, 41, pp.73-81. https://doi.org/10.1016/j.strusafe.2012.10.005

Ataei, N. and Padgett, J.E., 2013b. Probabilistic modeling of bridge deck unseating during hurricane events. Journal of Bridge Engineering, 18(4), pp.275-286. https://doi.org/10.1061/(ASCE)BE.1943-5592.0000371

Azadbakht, M. and Yim, S.C., 2015. Simulation and estimation of tsunami loads on bridge superstructures. Journal of Waterway, Port, Coastal, and Ocean Engineering, 141(2), p.04014031. https://doi.org/10.1061/(ASCE)WW.1943-5460.0000262

Azadbakht, M. and Yim, S.C., 2016. Estimation of Cascadia local tsunami loads on Pacific Northwest bridge superstructures. Journal of Bridge Engineering, 21(2), p.04015048. https://doi.org/10.1061/(ASCE)BE.1943-5592.0000755

Dassault Systèmes Simulia, 2021. Abaqus/Standard 2021. Dassault Systèmes Simulia, Providence, RI.

Kulicki, J.M., 2010. Development of the AASHTO guide specifications for bridges vulnerable to coastal storms. In Proc., 5th Int. Conf. on Bridge Maintenance, Safety and Management, IABMAS 2010 (pp. 2837-2844).

Padgett, J.E., Spiller, A. and Arnold, C., 2012. Statistical analysis of coastal bridge vulnerability based on empirical evidence from Hurricane Katrina. Structure and Infrastructure Engineering, 8(6), pp.595-605. https://doi.org/10.1080/15732470902855343

Pan, Y., Agrawal, A.K. and Ghosn, M., 2007. Seismic fragility of continuous steel highway bridges in New York State. Journal of Bridge Engineering, 12(6), pp.689-699. https://doi.org/10.1061/(ASCE)1084-0702(2007)12:6(689)

Pan, Y., Agrawal, A.K., Ghosn, M. and Alampalli, S., 2010. Seismic fragility of multispan simply supported steel highway bridges in New York State. I: Bridge modeling, parametric analysis, and retrofit design. Journal of Bridge Engineering, 15(5), pp.448-461. https://doi.org/10.1061/(ASCE)BE.1943-5592.0000085

Saeidpour, A., Chorzepa, M.G., Christian, J., Durham, S., 2018. Parameterized Fragility Assessment of Bridges Subjected to Hurricane Events Using Metamodels and Multiple Environmental Parameters. Journal of Infrastructure Systems, 24(4), DOI: 10.1061/(ASCE)IS.1943-555X.0000442

Yim, S. C., and Azadbakht, M., 2013. Tsunami forces on selected California coastal bridges. Technical Rep., Caltrans, Sacramento, CA.